An emerging PB2-627 polymorphism increases the pandemic potential of avian influenza virus by breaking through ANP32 host restriction in mammalian and avian hosts

Yuxin Guo[1], Sicheng Shu[1], Yong Zhou[1], Wenjing Peng[1], Zhimin Jiang[1], Yudong Li[1], Tian Li[1], Fanshu Du[1], Linlin Wang[1], Xue Chen[1], Jinze Dong[1], Chuankuo Zhao[1], Maggie Haitian Wang[2,3], Yipeng Sun[1], Honglei Sun[1], Lu Lu[4], Paul Digard[4], Kin-Chow Chang[5], Hui-Ling Yen[6], Jinhua. Liu[1*], Juan Pu[1*]

Affiliations:

[1] National key laboratory of Veterinary public health security, Key Laboratory for Prevention and Control of Avian Influenza and Other Major Poultry Diseases, Ministry of Agriculture and Rural Affairs, College of Veterinary Medicine, China Agricultural University; Beijing 100193, P.R. China.

[2] Centre for Clinical Research and Biostatistics, JC School of Public Health and Primary Care, the Chinese University of Hong Kong, Hong Kong SAR, China.

[3] CUHK Shenzhen Research Institute, Shenzhen, 518172, China.

[4] The Roslin Institute, University of Edinburgh, Edinburgh, EH25 9RG, United Kingdom.

[5] School of Veterinary Medicine and Science, University of Nottingham, Sutton Bonington Campus, Loughborough, LE12 5RD, UK.

[6] School of Public Health, Li Ka Shing Faculty of Medicine, The University of Hong Kong, Hong Kong Special Administrative Region, 999077, China.

*Corresponding author. Email: Juan Pu: pujuan@cau.edu.cn; Jinhua Liu: ljh@cau.edu.cn.

Abstract

Alterations in the PB2-627 domain could substantially increase the risk of an avian influenza virus (AIV) pandemic. So far, a well-known mammalian mutation PB2-E627K has not been maintained in AIV in poultry, which limits the spread of AIVs from avian to humans. Here, we discovered a variant, PB2-627V, which combines the properties of avian-like PB2-627E and human-like PB2-627K, overcoming host restrictions and posing a risk for human pandemics. Specifically, by screening the global PB2 sequences, we discovered a new independent cluster with PB2-627V emerged in the 2010s, which is prevalent in various avian, mammalian, and human isolates of AIVs, including H9N2, H7N9, H3N8, 2.3.4.4b H5N1, and other subtypes. And, the increasing prevalence of PB2-627V in poultry is accompanied by a rise in human infection cases with this variant. Then we systematically assessed its host adaptation, fitness, and transmissibility across three subtypes of AIVs (H9N2, H7N9, and H3N8) in different host models, including avian and human cells, chickens, mice, and ferrets where infections naturally occur. We found that PB2-627V facilitates AIVs to efficiently infect and replicate in chickens and mice by utilizing both avian- and human-origin ANP32A proteins. Importantly, and like PB2-627K, PB2-627V promotes efficient transmission between ferrets through respiratory droplets. Deep sequencing in passaged chicken samples and transmitted ferret samples indicates that PB2-627V remains stable across the two distinct hosts and has a high potential for long-term prevalence in avian species. Therefore, the mutation has the ability to continue spreading among poultry and can also overcome the barrier between birds and humans, greatly enhancing the likelihood of AIVs infecting humans. Given the escalating global spread of AIVs, it is crucial to closely monitor influenza viruses carrying PB2-627V to prevent a pandemic.

Author summary

Avian influenza viruses (AIVs) play a critical role in the evolution of pandemic influenza viruses. Adaptive changes in AIVs enable them to infect mammalian species by altering viral interactions with host-specific factors, and one well-known example is the PB2-E627K mutation. Fortunately, this mutation is sporadic and rare in AIVs, usually occurring after infecting humans, and AIVs with PB2-627E, which is prevalent in poultry, cannot easily infect humans. However, if an AIV manages to overcome this species barrier, the risk of a pandemic originating from an AIV will significantly increase. In our study, we identified a dual adaptive variant called PB2-627V that combines avian-like properties of PB2-627E and human-like properties of PB2-627K. This variant not only maintains viral fitness in chickens but also facilitates aerosol transmission of AIVs between ferrets. Mechanistically, PB2-627V utilizes both avian and human host protein ANP32A to support viral polymerase function. The mutation exhibited good fitness in both birds and humans, thereby greatly increasing the likelihood of AIVs infecting humans. The PB2-627V polymorphism has been found in birds, humans, and mammals worldwide across more than ten AIV subtypes. Given the escalating global spread of AIVs, we recommend considering PB2-627V as a new molecular marker to assess the pandemic potential of AIVs.

Introduction

Avian influenza viruses (AIVs) are critically important in the evolution of pandemic influenza viruses [1]. Adaptive changes in AIVs allow breakthrough infection in mammalian species through altering viral interactions with host-specific factors [2–4]. The current clade 2.3.4.4b highly pathogenic avian influenza (HPAI) H5Ny virus outbreaks have swept across continents, posing an unprecedented panzootic threat to birds, mammals, and public health [5] (https://www.who.int/news/item/12-07-2023-ongoing-avian-influenza-outbreaks-in-animals-pose-risk-to-humans). Other subtypes of AIVs have also been responsible for recurrent human infections [6]. For example, H7N7 [7], H7N9 [8,9], H10N8 [10], H5N6 [11], H10N3 [12] and H3N8 [13] viruses have caused over 1600 documented human cases [11]. Notably, most of these AIV subtypes possess internal (i.e. non-glycoprotein) genes that are derived from avian H9N2 viruses [8,11–13]. H9N2 virus is globally widespread in wild and domestic birds [14,15], and causes repeated human infections, especially since 2015. In these interspecies transmission events, critical adaptive mutations often occur on the PB2 protein of AIVs [12,16–19].

PB2 is one of three polymerase subunits of the influenza virus RNA-dependent RNA polymerase (RdRP), crucial for genome transcription and replication[20]. Specific amino acid changes have been identified in PB2 as key determinants of avian-to-mammalian adaptation, through its interaction with host acidic leucine-rich nuclear phosphoprotein 32 (ANP32) in avian and mammalian cells [21–24]. Their interactions exhibit host-species specificity[23]. PB2-627K in human influenza viruses interacts with human ANP32A and ANP32B (huANP32A and huANP32B) to support viral polymerase function [22]. On the other hand, PB2-627E in AIV can utilize avian ANP32A, but not huANP32A or huANP32B [22]. PB2-E627K amino acid substitution in AIVs promotes viral polymerase activity in mammalian cells by enhancing PB2

interaction with huANP32A and huANP32B [25]. Fortunately, the PB2-627K genotype is only frequently detected in AIVs isolated from human infections, and rarely detected in AIVs isolated from poultry or wild birds [26], greatly reducing the possibility of AIVs transmission to humans. In this study, we discovered an emerging PB2-627 polymorphism (PB2-627V) in diversified subtypes that increases the pandemic potential of AIVs by breaking through ANP32 host restriction in mammalian and avian hosts.

Results

PB2-627V prevalence in influenza virus isolates from avian and mammalian species

Given the crucial role of PB2 residue 627 in host adaptation, we analyzed 42,297 influenza PB2 sequences worldwide (excluding human H3N2 and H1N1pdm09 viruses) for polymorphisms at this position. We found that the number of sequences with PB2-627V rapidly increased after 2016 (Fig 1A). Among these viruses with PB2-627V, 71.3% were isolated from avian species, 14.7% were from humans, 14.0% were from other mammalian hosts (such as fox, swine, tiger, and mink) and environment (Fig 1A and S1 Table). In geographical distribution, 61.7% of the viruses were isolated in China, with the remaining (38.3%) found in the Middle East, Germany, Mexico, Canada, Italy, Spain, Russia, America, Denmark, and Belgium (Fig. 1A, and S1 Table). In terms of subtype distribution, 64.5% of PB2-627V variants were detected in H9N2 viruses, 9.9% in H7N9 and 9.1% in H5N6 viruses; the remaining 16.5% were in various other subtypes: H1N1, H1N2, H3N2, H3N8, H5N1, H5N2, H6N6, H7N1, and H10N3 (Fig. 1A, and S1 Table). Notably, PB2-627V has also been identified in clade 2.3.4.4b H5N1 viruses isolated from wild birds and red foxes (Fig. 1A, and S1 Table).

107 In phylogenetic analysis, recent PB2-627V sequences mainly belong to a major group that
108 includes most human and avian isolates from multiple subtypes (H9N2, H7N9, H5N6, H3N8,
109 H10N3, and H5N1 viruses) (Fig 1B). For H9N2 subtype, PB2 gene showed the evolution of a
110 PB2-627V cluster (S1A Fig). Ancestral host reconstruction on time-scaled phylogeny indicated
111 that chicken isolates are the origin of human isolates within this cluster (S1B Fig). Notably,
112 PB2-627V of H9N2 is more frequently detected in humans than avian isolates from 2016-2022
113 (Fig 1C). Similarly, there was a dramatic increase in PB2-627V detection in avian and human
114 hosts for the H7N9, H5N6, and H3N8 subtypes after 2016 (S2 Fig). Thus, it appears that
115 PB2-627V has achieved better adaptability in poultry populations and its emerging prevalence
116 both in avian and humans suggests functional significance across various host species.

117 PB2-627V promotes polymerase activity of H9N2 AIV in human and 118 chicken cells by utilizing ANP32 proteins of both host species

119 To evaluate the functionality of PB2-627V, we used a previously identified chicken H9N2
120 isolate A/chicken/Hubei-m0530/2017 (referred to as 17/H9N2^{627E}) with PB2-627E as the
121 backbone, and introduced the PB2-E627V and PB2-E627K changes. Although PB2-627V and
122 -627K are found in other natural chicken isolates, this approach allowed the dissection of the
123 function of this single mutation. A dual-luciferase assay system was used to compare viral
124 polymerase activities conferred by PB2-627E, V, and K in avian DF-1 cells and human 293T
125 cells at 33°C and 37°C, respectively, mimicking the temperature of human upper and lower
126 respiratory tract [27]. In DF-1 cells, 17/H9N2^{627E}, 17/H9N2^{627V}, and 17/H9N2^{627K} showed
127 comparable polymerase levels at 33°C and 37°C (Fig 1D). However, a 23.6-fold (±2.6) increase
128 in polymerase activity at 33°C, and an 11.8-fold (±0.6) increase at 37°C were found with

129 17/H9N2^{627V} in 293T cells compared with 17/H9N2^{627E} ($p < 0.001$); 17/H9N2^{627K} exhibited a
130 9.3-fold (±2.6) increase in polymerase activity at 33°C and a 20.2-fold (±0.4) increase at 37°C (p
131 < 0.001) relative to 17/H9N2^{627E} (Fig. 1E). Accordingly, in avian DF1 cells, PB2-627V
132 demonstrated more robust viral transcriptional and replication functions than PB2-627K, while in
133 human A549 cells, it surpassed PB2-627E (S3A and S3B Fig).

134 Viral polymerase activity was further examined in ANP32A and ANP32B double-knockout
135 293T (DKO) cells over-expressing chicken- or human-ANP32 protein(s) [25]. As expected,
136 polymerase activities of all 3 viruses (17/H9N2^{627E}, 17/H9N2^{627V}, and 17/H9N2^{627K}) in control
137 DKO cells were significantly lower than those in the wild type 293T cells (S3C Fig). Polymerase
138 activity of 17/H9N2^{627E} in the DKO cells was significantly enhanced in the presence of chicken
139 ANP32A (chANP32A) at both 33°C and 37°C ($p < 0.05$) (Fig 1F). With 17/H9N2^{627V},
140 chANP32A in DKO cells significantly enhanced the polymerase activity at both 33°C and 37°C
141 ($p < 0.05$), and huANP32A significantly enhanced polymerase activity only at 37°C ($p < 0.001$)
142 (Fig 1F). With 17/H9N2^{627K}, expression of chANP32A in DKO cells significantly enhanced viral
143 polymerase activity only at 37°C ($p < 0.001$), and huANP32A and huANP32B significantly
144 enhanced the polymerase activity at both 33°C and 37°C ($p < 0.001$) (Fig 1F).

145 ANP32 interface with PB2 at the 627-domain by electrostatic and hydrophobic interactions
146 [28]. PB2-627K (lysine) has a positive charge and PB2-627E (glutamic acid) has a negative
147 charge. Modeling the surface electrostatic potential predicted that valine at PB2-627 confers a
148 neutral state (Fig 1G), which could permit the PB2 protein to interact sufficiently with avian and
149 human ANP32A proteins to promote viral polymerase activity in avian and human cells. In
150 summary, these findings indicate that PB2-627V can utilize chicken and human ANP32A in the
151 respective species of cells to facilitate viral polymerase activity.

152 **PB2-627V in H9N2 virus maintains efficient replication in chickens**

153 **and facilitates replication in human cells and mice**

154 Next, viruses with the three PB2 627 polymorphisms were rescued on the background of the
155 17/H9N2 virus. The replication kinetics of these 17/H9N2^{627E}, 17/H9N2^{627V}, and 17/H9N2^{627K}
156 viruses were assessed in avian CEF cells; no significant differences in replication were found
157 between viruses ($p > 0.05$) (Fig 2A). Chickens individually inoculated with 10^6 EID_{50} of each
158 virus showed no mortality (S4A Fig) and no apparent clinical signs. Viral loads detected from
159 oropharyngeal swabs of 17/H9N2^{627V} and 17/H9N2^{627E} inoculated chickens were significantly
160 higher than those infected with 17/H9N2^{627K} at 6 and/or 8 dpi ($p < 0.05$) (Fig 2B). The three
161 viruses replicated to comparable titers in the turbinates at 3 dpi, but 17/H9N2^{627V} replicated to
162 higher titers than 17/H9N2^{627K} in the lungs ($p < 0.05$) (Fig 2C). Histopathological examination of
163 chicken lungs at 3 dpi indicate that all viruses induced inflammatory responses, with more
164 hemorrhage noted in 17/H9N2^{627V} infected lungs (Fig 2D). These findings indicate that
165 PB2-627V and PB2-627E replicated comparably well in chickens.

166 In infected human A549 cells, virus titers of 17/H9N2^{627V} and 17/H9N2^{627K} were
167 significantly higher than that of 17/H9N2^{627E} from 12 to 48 hpi ($p < 0.001$); there was no
168 significant difference between 17/H9N2^{627V} and 17/H9N2^{627K} ($p > 0.05$) (Fig 2E). Mice
169 inoculated with 17/H9N2^{627E}, 17/H9N2^{627V}, or 17/H9N2^{627K} virus, showed no obvious clinical
170 signs, as in infected chickens (Fig 2F and S4B Fig). Higher virus loads were detected in the nasal
171 turbinates and lungs of mice infected with 17/H9N2^{627V} and 17/H9N2^{627K} at 3 dpi than those with
172 17/H9N2^{627E} ($p < 0.001$); there was no significant difference in virus titers between the
173 17/H9N2^{627V} and 17/H9N2^{627K} groups ($p > 0.05$) (Fig 2G). Likewise, 17/H9N2^{627V} and

174 17/H9N2^{627K} viruses produced more viral NP protein-positive cells in the lung than in
175 corresponding 17/H9N2^{627E} infected mice (Fig 2H). Thus, the infectivity of PB2-627V H9N2
176 virus in human cells and mice is similar to that of PB2-627K virus.

177 PB2-627V confers aerosol transmission of H9N2 virus in ferrets

178 Transmissibility of influenza viruses between ferrets is an indicator of potential epidemic or
179 pandemic risk. Direct contact (DC) and respiratory droplet (RD) transmission tests of the
180 17/H9N2^{627E}, 17/H9N2^{627V}, and 17/H9N2^{627K} viruses were performed in ferrets. All viruses
181 infected the directly infected donor animals, as assessed by virus titers in nasal washes (Fig.
182 3A-3C, and S2 Table). 17/H9N2^{627V} and 17/H9N2^{627K} viruses were transmitted to all DC ferrets
183 and all RD ferrets, but 17/H9N2^{627E} was only transmitted to DC groups. Transmission by RD in
184 the 17/H9N2^{627V} group took place around 2 days later than in the 17/H9N2^{627K} group (Fig
185 3A-3C). Areas under the curve (AUC), based on virus titers over time in the nasal washes, were
186 determined to compare total viral shedding during infection (Fig 3D and S3 Table). In donor
187 ferrets, virus production was comparable between the three viruses. In DC ferrets, 17/H9N2^{627V}
188 virus output (AUC = 18.13 ± 3.69) was slightly higher than that of 17/H9N2^{627E} virus (14.13 ±
189 3.01, $p = 0.19$) and 17/H9N2^{627K} virus (16.25 ± 1.27, $p = 0.68$). In RD ferrets, 17/H9N2^{627V} virus
190 output (AUC = 11.75 ± 2.88) was slightly lower than that of 17/H9N2^{627K} virus (15.42 ± 1.60, p
191 = 0.25) (Fig 3D and S3 Table). Thus, in contrast to PB2-627E, PB2-627V promotes aerosol
192 transmissibility of H9N2 virus in ferrets.

193 To monitor any polymorphic changes at residue PB2-627 during virus infection and
194 transmission, next-generation sequencing was performed on nasal wash samples from each ferret
195 at the first and the last time points of positive virus detection. In 17/H9N2^{627E} groups, 627E
196 remained the dominant genotype in the donors and DC ferrets (Fig 3E). In the donor groups of

197 17/H9N2^{627V} and 17/H9N2^{627K}, 627V and 627K were the corresponding dominant genotypes. In
198 the DC and RD transmission groups of 17/H9N2^{627V} and 17/H9N2^{627K}, polymorphisms at
199 PB2-627 during infection were more noticeable, but at the last detection time point of each RD
200 group, corresponding 627V and 627K returned to their earlier dominance (Fig 3F and 3G). These
201 results suggest that residue PB2-627V stably confers aerosol transmission of H9N2 virus in
202 ferrets.

203 PB2-627V has the potential for sustained prevalence in poultry

204 17/H9N2^{627E}, 17/H9N2^{627V}, and 17/H9N2^{627K} H9N2 viruses were serially passaged in
205 chickens to assess the potential for sustained prevalence of PB2-627V in poultry. Chickens were
206 directly infected with each virus (Passage 1, P1) and subsequently (P2 - P5) passaged through
207 contact transmission (Fig 4A). All viruses were successfully passaged from P1 to P5. We then
208 performed next-generation sequencing of whole viral genomes from RNA isolated from the
209 lungs of the P5 chickens. Mutations above 1% threshold were identified as intra-host single
210 nucleotide variants (iSNVs) [29,30]. Overall, most iSNVs were detected at low frequency and
211 there were no significant differences between the 3 groups (Fig 4B). Notably, variant frequency
212 at residue PB2-627 was below the 1% threshold in all P5 chicken samples (Fig 4C). At the
213 amino-acid level, two variant residues (PA-D529N, NP-T211D) occurred at a high frequency
214 (>10%) in the 17/H9N2^{627K} group, but no high-frequency variant residues were detected in
215 17/H9N2^{627E} and 17/H9N2^{627V} groups (Fig 4D), suggesting that compared to PB2-627E and
216 PB2-627V, PB2-627K required other cooperative mutations in RNP genes for transmission in
217 chickens. Taken together, PB2-627V showed a high potential for sustained prevalence in
218 chickens.

PB2-627V confers dual ability to replicate in chickens and mice to avian H7N9 and H3N8 viruses

We determined if the dual host adaptability of PB2-627V, detected at high frequency in the H9N2 virus, is transferrable to other AIV subtypes. H7N9 and H3N8 viruses possess the PB2 gene and other internal genes derived from the H9N2 viruses [9,31]. The natural mutations PB2-E627V and PB2-E627K were separately introduced into the LPAI H7N9 (A/chicken/China/0606-12/2017, referred as 17/H7N9^{627E}) and H3N8 (A/chicken/Anhui/FE12/2022, referred as 22/H3N8^{627E}) [32] viruses. The resulting PB2-627V, PB2-627K, and PB2-627E viruses were assessed for replication and pathogenicity in chickens and mice.

In chickens, introduction of PB2-E627V or PB2-E627K mutation into 17/H7N9 and 22/H3N8 viruses did not significantly affect replication or pathogenicity relative to their PB2-627E counterparts (Fig 5A-5E), although the replication of 17/H7N9^{627V} in chicken lungs was significantly higher than that of 17/H7N9^{627K} ($p<0.05$) (Fig 5B). Thus, PB2-E627V had little effect on virus replication and pathogenicity in chickens (Fig. 5A-5E, and S5A Fig). In mice, both PB2-E627V and PB2-E627K changes in 17/H7N9 and 22/H3N8 viruses led to virus loads in the nasal turbinates and lungs, weight loss, and mortality ($p<0.01$) (Fig 5F-5K). Murine lungs at 3 dpi. with subtypes housing PB2-627V showed more severe pathology than those with PB2-627E (Fig 5L for 17/H7N9 and S5B Fig for 22/H3N8). In summary, PB2-E627V significantly increases pathology and replication of H7N9 and H3N8 virus subtypes in mice and maintains their replication fitness in chickens.

240 # Discussion

241 Here, we identified PB2-627V as an emerging variant in AIVs with significant zoonotic and
242 pandemic potential. We observed that PB2-627V enhances the polymerase activity of H9N2 AIV
243 in both human and chicken cells by utilizing ANP32A proteins from both species, thereby
244 overcoming the restriction imposed by human ANP32 on AIVs carrying PB2-627E and
245 exhibiting properties similar to those with PB2-627K. PB2-627V in H9N2 virus maintains
246 efficient replication in chickens, facilitates virus replication in mice, and confers aerosol
247 transmission in ferrets. Furthermore, PB2-627V is stably maintained in passages through
248 chickens and also conferred the dual ability to replicate in chickens and mice to avian H7N9 and
249 H3N8 subtype viruses. Thus, the increased prevalence of this dual adaptive mutation of
250 PB2-E627V in poultry greatly increases the chances of AIVs infecting humans. In addition, the
251 wide distribution of this mutation in multiple subtypes, hosts, and countries poses global public
252 health risks.

253 Clinical data and phylogenetic analysis revealed that residue PB2-627V originated in
254 chicken influenza viruses (likely the H9N2 subtype) and was subsequently transmitted to humans.
255 The prevalence of PB2-627V in AIVs is on the rise, particularly within the H9N2 subtype, and
256 PB2-627V is also found in other subtypes such as H7N9, H5N6, H3N8, and H10N3, which
257 contain reassorted internal genes derived from H9N2 [8,11–13]. Serial passage studies in
258 chickens further indicate that additional mutations occurred in the polymerase protein after the
259 passage of H9N2 viruses with the PB2-E627K. However, H9N2 viruses with PB2-627E and
260 -627V did not produce further mutations. This may be due to the PB2-627K mutation still having
261 defects in transmission in chickens and requiring further adaptation. This could explain why
262 PB2-627K is very rare in avian isolates. The PB2-E627K mutation usually takes place in

263 infected humans [33]. Conversely, PB2-627V appears to be a product of evolution in H9N2 virus
264 and has a high potential for long-term prevalence in poultry populations, posing an increasing
265 likelihood of viral transmission to humans.

266 Cellular ANP32 proteins specifically support influenza virus genome replication. ANP32A
267 can bridge PB2 dimers and form extensive contacts with two polymerases to maintain a dimeric
268 assembly [22,34]. The C-terminal low complexity acidic region (ANP32A^{LCAR}) inserts between
269 two PB2-627 domains of the polymerase dimer. Human ANP32A^{LCAR} contains only acidic
270 amino acid residues. Thus, with human ANP32A, basic or uncharged residues (such as lysine, K
271 or valine, V) are preferred in the PB2-627 domain to acidic amino acids (such as glutamic acid,
272 E) [21,22]. In avian cells, the additional 33 amino acids in chANP32A^{LCAR} allow AIVs carrying
273 PB2-627E to effectively utilize chANP32A in avian cells [23,35]. Indeed, in the context of
274 H9N2, we found that the polymerase activity of PB2-627V in avian cells is comparable to
275 PB2-627E, and in human cells is comparable to PB2-627K which suggests that the nonpolar
276 neutral amino acid of PB2-627V has the dual ability to interact with avian ANP32A and human
277 ANP32A in different host cells. It is noteworthy that, when the PB2-627 site is changed from E
278 to V, the virus can not only undergo contact transmission in ferrets but also undertake effective
279 aerosol transmission, similar to that of the 17/H9N2^{627K} variant. In addition, PB2-627V can be
280 maintained in ferret post-infection, during contact and aerosol transmission. Thus, these features
281 suggest that the dual adaptive PB2-627V AIVs reduce the host barrier between avians and
282 humans.

283 The PB2-E627V has been identified in H5N1 viruses where it was shown to increase viral
284 replication in mammalian cells and virulence in mice [36], while in the background of a
285 laboratory strain of H1N1 (PR8), it reduced viral replication in mammalian cells compared with

286 PB2-627K [37]. However, because the PB2-627V variant was rarely found in natural influenza
287 isolates at that time (before 2015), it did not attract much attention. In H9N2 AIVs, PB2-627V
288 variants appeared in the Middle East from 2000 to 2015 but were not stably maintained. The
289 genotype of Middle East H9N2 viruses was very different from the G57 lineage [8] H9N2 virus
290 prevalent in China and studied here [38,39]. Under experimental conditions, PB2-627V in the
291 Middle East H9N2 virus needs to operate in concert with PB2-E543D, PB2-A655V and
292 PB2-K526R to enhance viral replication in mammals [38]. Numerous adaptive mutations have
293 recently been identified in the G57 H9N2 virus, including PB2-292, PB2-588, PA-356, M1-37
294 and HA-226 [15,40,41], in avian and human isolates [42–45]. It is plausible that one or more of
295 these adaptive changes in the G57 genotype exert epistatic effects to induce the emergence of the
296 stable PB2-627V residue, but this remains to be tested.

297 Collectively, our results suggest that the recent evolved variant PB2-E627V combines the
298 characteristics of avian-like PB2-627E and human-like PB2-627K. It exhibits a crucial
299 dual-adaptation that can effectively infect and transmit in both avian and mammalian hosts,
300 thereby overcoming the interspecific barrier between birds and humans. The presence of
301 PB2-627V in multiple subtypes of AIVs undoubtedly escalates the risk of an avian influenza
302 virus pandemic. We therefore recommend considering PB2-627V as a new molecular marker to
303 assess the pandemic potential of AIVs.

304 Materials and Methods

305 Ethics statement

306 9 to 11-day-old specific pathogen-free (SPF) embryonated chicken eggs and all
307 experimental animals were purchased from Boehringer Ingelheim, China. All animal research

308 was approved by the Beijing Association for Science and Technology (approval ID SYXK,
309 Beijing, 2020-0053) and performed in compliance with the Beijing Laboratory Animal Welfare
310 and Ethics guidelines, as issued by the Beijing Administration Committee of Laboratory Animals,
311 and by the China Agricultural University (CAU) Institutional Animal Care and Use Committee
312 guidelines (ID: SKLAB-B-2010-003) approved by the Animal Welfare Committee of CAU. The
313 H9N2, H7N9, and H3N8 wild-type viruses used are all low pathogenic avian influenza (LPAI)
314 viruses isolated from chickens. PB2-E627V and PB2-E627K are natural mutations found in these
315 viruses.

316 **Sequence collection and alignment**

317 The sequences of the PB2 gene were obtained from the GISAID database
318 (http://www.gisaid.org). After removing the PB2 sequences of human H3N2 and H1N1pdm09
319 viruses and duplicate sequences, a total of 42,297 full-length PB2 sequences of IAVs published
320 globally from 1994 to 2022 were obtained. All accession codes of public sequences can be found
321 in Dataset S1. Sequences were aligned using MUSCLE v3.7 [46] via the CIPRES Science
322 Gateway [47].

323 **Phylogenetic analyses**

324 The phylogenetic tree of the H9N2 PB2 gene was constructed using a total of 4523 PB2
325 sequences from H9N2 subtype IAVs. The phylogenetic tree of PB2-627V was constructed using
326 a total of 394 PB2 sequences carrying the PB2-627V. IQ-TREE version 1.6 was used to
327 construct the maximum likelihood phylogenetic trees, applying the best-fit general
328 time-reversible model of nucleotide substitution with gamma-distributed rate variation among
329 sites (GTR + I + G), and performing ultrafast bootstrap resampling analysis (1000 replications).

330 Phylogenetic trees were visualized and annotated using FigTree version 1.4.4, Adobe Illustrator
331 2021, and Interactive Tree Of Life (iTOL) [48].

332 Host transmission dynamics analyses

333 A maximum clade credibility (MCC) tree was performed on the PB2-627V cluster
334 sequences (Fig. S1A) with BEAST v1.10.4. Using the coalescent Bayesian Skygrid model, the
335 General Time Reversible (GTR) model of evolution and the strict clock were employed. The
336 host jump patterns were interfered by mapping the host types onto the time-scaled tree using an
337 asymmetric discrete trait model [49]. A Markov Monte Carlo (MCMC) chain is run for 30
338 million, sampled every 3000 and the first 10% of tree was removed as burn-in. Stationarity and
339 mixing were checked with Tracer v1.7.2. The MCC tree was finally generated by TreeAnnotator
340 and visualized using FigTree v1.4.4.

341 PB2 protein structure simulation

342 A simulation of the A/chicken/Hebei/m0530-1/2017 (17/H9N2) PB2 protein structure was
343 performed by using Swiss-Model (https://swissmodel.expasy.org). The 17/H9N2 PB2 protein
344 sequence was inputted in FASTA format, and the published H7N9 protein structure (PDB:
345 7qtl.1.C) with 98.94% sequence identity was utilized as the template. The quality of the resulting
346 model was evaluated using GMQE and QMEAN scores. PyMOL was utilized to introduce the
347 PB2-E627V and PB2-E627K mutations into the model and to ascertain the surface charge of the
348 protein.

349 Cell lines

350 Human lung epithelial cell (A549) cells, kidney epithelial (293T) cells, chicken fibroblast
351 (DF-1) cells, and Madin-Darby Canine Kidney (MDCK) cells were maintained in our laboratory.

352 Chick embryo fibroblast (CEF) cells were obtained from SPF embryonated chicken eggs as
353 previously described [50]. 293T cell line with a double knockout of ANP32A and ANP32B
354 (DKO cell) was kindly provided by Xiaojun Wang from Harbin Veterinary Research Institute.
355 Cells were cultured with Dulbecco's modified Eagle medium (DMEM; Gibco, New York, USA)
356 supplemented with 10% fetal bovine serum (FBS; Gibco, Sydney, Australia) and 1%
357 penicillin-streptomycin solution (MACGENE, Beijing, China).

358 **Influenza viruses**

359 H9N2 AIV A/chicken/Hebei/m0530-1/2017 (17/H9N2) was characterized and maintained
360 in our laboratory. Influenza H7N9 virus A/chicken/China/0606-12/2017 (17/H7N9) and
361 influenza H3N8 virus A/chicken/Shandong/FE12/2022(H3N8) (22/H3N8) were isolated by our
362 laboratory. Viruses were propagated in 9 to 11-day-old SPF embryonated chicken eggs at 35°C
363 for 72 hours. Virus titers were determined by 50% tissue culture infectious dose ($TCID_{50}$) on
364 MDCK cells or 50% egg infectious dose (EID_{50}) on SPF chicken eggs.

365 **Animals**

366 5 to 6 weeks-old female SPF BALB/c mice and 6 to 8 weeks-old female SPF chickens were
367 purchased from Vital River Laboratory Animal Technology Co., Ltd (Beijing, China). Mice were
368 kept in individually ventilated cages (IVC), and chickens were kept in high efficiency particulate
369 air (HEPA)-filter isolators in the Animal Care Facilities at CAU. Five to six-month-old male
370 Angora ferrets (*Mustela putorius furo*), serologically negative for currently circulating influenza
371 viruses (H1, H3, H5, H7, and H9) and > 1.0 kg (ranging from 1.10 to 1.80 kg) in weight, were
372 purchased from Angora LTD (Jiangsu, China). All ferrets were housed in wire cages placed
373 inside HEPA-filter isolators. All animals were allowed free access to water and a standard chow

374 diet, and provided with a 12-hour light and dark cycle (temperature: 20-25°C, humidity:
375 40%-70%). All animals used were not involved in any other experimental procedure.

376 Generation of viruses by reverse genetics

377 As described previously [18], recombinant viruses were generated using a plasmid-based
378 reverse genetics system in the genetic background of 17/H9N2, 17/H7N9, and 22/H3N8.
379 Mutations were introduced into the plasmids using PCR-based site-directed mutagenesis. To
380 check for the absence of unintended mutations, all propagated viruses were subjected to
381 complete sequencing.

382 Polymerase activity assay

383 To compare the polymerase activities of different viral ribonucleoprotein (RNP) complexes,
384 a dual-luciferase reporter assay system (Promega, Madison, WI, USA) was employed [25]. The
385 PB2, PB1, PA, and NP gene segments of respective viruses were individually cloned into the
386 pCDNA3.1 expression plasmid. 125 ng of each of the PB2, PB1, PA, and NP plasmids, as well
387 as 10 ng of the pLuci luciferase reporter plasmid and 2.5 ng of the Raniera internal control
388 plasmid, were transfected into 293T cells or DF-1 cells. The cell cultures were then incubated at
389 33°C or 37°C for 24 hours. The transfected cells were then lysed and analyzed for firefly and
390 renilla luciferase activities using a GloMax 96 microplate luminometer (Promega). The function
391 of ANP32 was examined using a polymerase assay by co-transfection of DKO cells with
392 different ANP32 proteins or empty vector (20 ng) at 33°C or 37°C for 24 hours. All of the
393 experiments were performed independently at least three times.

394 ## Growth kinetics of viruses in A549 and CEF cells

395 A549 and CEF cells were cultured in 6-well plates and infected in triplicate with indicated
396 viruses at a multiplicity of infection (MOI) of 0.1 (A549) or 0.01 (CEF). After a 2-hour
397 incubation, cells were washed three times with DPBS, and incubated at 37°C in 5% CO_2.
398 Supernatants were collected at 12, 24, 36, 48, and 60 hours post-infection (hpi), and virus titers
399 were determined by $TCID_{50}$ assays on MDCK cells.

400 ## Quantitative real-time PCR assay

401 Levels of mRNA and viral RNA (vRNA) were determined in A549 cells and DF-1 cells
402 infected in triplicate with viruses (17/H9N2^{627E}, 17/H9N2^{627V}, or 17/H9N2^{627K}) at an MOI of
403 0.1(A549 cells) or MOI of 0.001 (DF-1 cells). Total RNA was extracted from infected cells by
404 using TRIzol reagent according to the manufacturer's instructions (Invitrogen). For the detection
405 of mRNA and vRNA, the oligo(dT) primer and primer uni-12 (5'- AGCAAAAGCAGG -3')
406 were used respectively to generate cDNAs from 1 μg of total RNA per sample by using
407 Superscript III first-strand synthesis supermix (Invitrogen). The quantitative real-time PCR
408 (qRT-PCR) mixture for each reaction sample consisted of 10 μL of 2× SYBR green PCR master
409 mix (Applied Biosystems), 7 μL of nuclease-free water, 0.5 μL of each primer, and 2 μL of the
410 cDNA template. qPCR was conducted using a 7500 real-time PCR system (Applied Biosystems)
411 with the following program: 1 cycle at 95°C for 10 min, followed by 40 cycles of 95°C for 15 s
412 and 60°C for 1 min. Expression values for each gene, relative to *β-actin*, were calculated by
413 using the $2^{-\Delta\Delta CT}$ method. Each qPCR sample contained three technical replicates. Primers for the
414 amplification of the *β-actin* and PB2 genes are as follows: forward primer
415 5'-AGAGCTACGAGCTGCCTGAC-3' and reverse primer 5'-CGTGGATGCCACAGGACT-3'

416 for *β-actin*, forward primer 5'- GGAACAGGAATGGACCGACA-3' and reverse primer
417 5'-ACTGAGATCTGCATGACCCG-3' for PB2.

418 Mouse challenge studies

419 Groups of eight mice were anesthetized by intramuscular injection of Zoletil 50 (Zoletil;
420 Virbac SA, Carros, France) at a dose of 20 mg/kg, and inoculated intranasally (i.n.) with 10^6
421 $TCID_{50}$ of test virus or PBS in a total volume of 50 μL. At 3 days post-infection (dpi), 3 mice
422 from each group were euthanized, and lung and nasal turbinate tissues were collected for virus
423 titration in MDCK cells by $TCID_{50}$ assay. Lungs of mice infected with the indicated viruses at 3
424 dpi were collected for histopathology and immunohistochemistry (IHC). The remaining 5
425 animals were monitored in the remaining two weeks for disease progression, weight change, and
426 mortality. Mice that experienced a weight loss exceeding 25% of their original weight were
427 humanely euthanized.

428 Chicken challenge studies

429 Experimental procedures for virus infection of chickens were under previously described
430 protocol [51]. Groups of 6 chickens were inoculated i.n. with 10^6 EID_{50} of indicated virus or PBS
431 in a volume of 200 μL. At 3 dpi, 3 chickens from each group were euthanized, and lung and
432 nasal turbinate tissues were collected for virus titration by EID_{50} assay. Lungs of chickens at 3
433 dpi were collected for histopathology and IHC. The remaining 3 chickens were monitored and
434 tracheal swabs were taken at 2, 4, 6, and 8 dpi for virus titration by EID_{50} assay.

435 Histopathology and IHC analysis

436 Lungs were fixed in 10% buffered formalin, embedded in paraffin, sectioned and stained
437 with hematoxylin and eosin (H&E). Tissue sections were also immunostained with a viral NP

438 monoclonal primary antibody (ab20343, Abcam, Beijing, China). The secondary antibody used
439 was conjugated to horse radish peroxidase (HRP), and the color reaction was based on the use of
440 an HRP reaction kit (ZSGB-BIO, Beijing, China). Histopathological examination was conducted
441 blind by two experienced experimental pathologists.

442 Virus passage in chickens

443 For virus passage in chickens, as depicted in Fig. 4A, groups of 2 SPF chickens were
444 inoculated at passage 1 (P1) with 10^6 EID_{50} of the indicated virus in a volume of 200 μL. At 3
445 dpi, 2 naïve chickens were co-housed with the P1 chickens to establish the P2 generation. At 6
446 dpi of P1 chickens, lung tissues of P1 chickens were collected and homogenized in 500 μL of
447 cold PBS, and another 2 naïve chickens were introduced as P3. The same sequential steps were
448 used for passage up to the P5.

449 Ferret transmission experiments

450 The transmission study consisted of groups of 3 ferrets, following a previously described
451 protocol[32,52] comprising one infected, one direct contact (DC), and one respiratory droplet
452 contact (RD) group. Ferrets were housed in wire cages inside isolators, with each isolator
453 approximately 15 cubic feet in size. Each ferret was sedated with ketamine (20 mg/kg) and
454 xylazine (1 mg/kg) via intramuscular injection and inoculated intranasally with 10^6 $TCID_{50}$ of
455 17/H9N2^{627E}, 17/H9N2^{627V}, or 17/H9N2^{627K} virus in a volume of 500 μL delivered at 250 μL per
456 nostril. Twenty-four hours later, 2 naïve ferrets were introduced into the isolator, with the direct
457 contact ferret placed in the same cage as the infected ferret, while the respiratory droplet contact
458 ferret was placed in a cage separated by a wire mesh wall to prevent physical contact.

459 Individual weight was monitored throughout the study. Nasal washes were collected from
460 the ferrets by 2 mL virus transport medium every other day for 14 days and titrated for viruses in
461 MDCK cells by TCID50 assays. Additionally, 200 μL nasal washes were used for RNA
462 extraction and deep sequencing. At 21 dpi, blood samples of ferrets were collected to determine
463 seroconversion using the HI Assay.

464 Next generation sequencing

465 A total of 54 ferret nasal wash samples, 6 chicken lung samples, and 3 viruses (17/H9N2^{627E},
466 17/H9N2^{627V}, and 17/H9N2^{627K}) were subjected to whole-genome sequencing. Viral RNA was
467 harvested from the samples by using the QIAamp Viral RNA Mini Kit (Qiagen). Multiplex
468 reverse transcription-PCR amplification of all 8 influenza virus genome segments was performed
469 on RNA samples using PrimeScript™ II 1st Strand cDNA Synthesis Kit (Takara 6210) and
470 primers Uni12/Inf1 (5'-GGGGGGAGCAAAAGCAGG-3'), Uni12/Inf3
471 (5'-GGGGGAGCGAAAGCAGG-3'), and Uni13/Inf1
472 (5'CGGGTTATTAGTAGAAACAAGG-3'). As previously described [32], PCR products were
473 purified on spin columns and quantified by using the Quant-It Pico Green kit (Invitrogen,
474 Carlsbad, USA). The purified amplicons were pooled in equimolar and paired-end sequenced
475 (23150) on an Illumina NovaSeq platform according to the standard protocols. Sequencers by
476 200 or 250 bp paired-end sequencing, and sequencing depth for avian influenza virus isolates
477 was about 0.2 G per sample. NGS findings were validated by qRT-PCR. Raw NGS reads were
478 processed by filtering out low-quality reads (eight bases with quality < 66), adapter-contaminated
479 reads (with > 15 bp matched to the adapter sequence), poly-Ns (with 8 Ns), duplication and
480 host-contaminated reads (SOAP2 [version 2.21]; less than five mismatches). Sanger sequences of
481 parental viruses were chosen as reference sequences. Burrows-Wheeler Alignment Tool (version

482 0.7.12) and SAMtools (version 1.4) were then used to perform reference-based assembly. Data
483 analyses were performed using a custom quality-based variant detection pipeline.
484 To detect the genomic variants, the iSNVs were identified as following standards: 1) reads
485 > 1000; 2) mutation rates >1%. The iSNVs frequency was calculated by using the number of
486 iSNVs divided by the total number of genome sites.

487 Quantification and statistical analysis

488 Graphing and statistical analyses were performed using GraphPad Prism 8 (GraphPad
489 Software, San Diego, California, USA; www.graphpad.com). Experimental groups were
490 statistically compared by analysis of variance (ANOVA). P value < 0.05 was considered to
491 indicate statistical significance.

492 Acknowledgments

493 We thank the Global Initiative on Sharing Avian Influenza Data (GISAID) for sharing the
494 influenza virus sequence data used in this study. We are grateful to Xiaojun Wang (Harbin
495 Veterinary Research Institute, China) for providing the DKO cells, Shangang Jia (China
496 Agricultural University, China) for helpful suggestions on data analysis, and Nianzhi Zhang
497 (China Agricultural University, China) for constructive suggestions on structure analysis. We
498 thank BioRender (biorender.com) for assisting with graphics.

499 Funding

500 National Key Research and Development Program of China 2022YFF0802403 (JP)
501 National Key Research and Development Program of China 2021YFD1800202 (JP)
502 National Natural Science Foundation of China 32192450 to (JL)
503 National Natural Science Foundation of China 32102661 (ZJ)

UK Biotechnology and Biological Sciences Research Council BBS/E/D/20002173 (PD and LL)

Author contributions

Research designing: JP, YG

Data collection and analysis: YG, YZ, YL

Experiment: YG, TL, LW, XC, JD, CZ, FD

Funding acquisition: JP, JL, ZJ, PD, LL

Writing – original draft: YG, JP

Writing – review & editing: JL, HLY, LL, PD, KCC, MHW, HS, YS, ZJ, FD

Competing interests

The authors declare that they have no competing interests.

Data and materials availability

Genetic variation data of H9N2 viruses during passage in chickens are available at Mendeley data (DOI: 10.17632/zpvwwj59kx.1). All other data supporting the findings of this study are available w in the main text or the supplementary materials.

References

1. Krammer F, Smith GJD, Fouchier RAM, Peiris M, Kedzierska K, Doherty PC, et al. Influenza. Nat Rev Dis Primers. 2018;4: 3. doi:10.1038/s41572-018-0002-y

2. Amat JAR, Patton V, Chauché C, Goldfarb D, Crispell J, Gu Q, et al. Long-term adaptation following influenza A virus host shifts results in increased within-host viral fitness due to higher replication rates, broader dissemination within the respiratory epithelium and reduced tissue damage. PLoS Pathog. 2021;17: e1010174. doi:10.1371/journal.ppat.1010174

3. Su W, Harfoot R, Su YCF, DeBeauchamp J, Joseph U, Jayakumar J, et al. Ancestral sequence reconstruction pinpoints adaptations that enable avian influenza virus transmission in pigs. Nat Microbiol. 2021;6: 1455–1465. doi:10.1038/s41564-021-00976-y

4. Wang J, Samaan M. Tool for Influenza Pandemic Risk Assessment - version 2. : 65.

5. European Food Safety Authority, European Centre for Disease Prevention and Control, European Union Reference Laboratory for Avian Influenza, Adlhoch C, Fusaro A, Gonzales JL, Kuiken T, Melidou A, et al. Avian influenza overview April – June 2023. EFS2. 2023;21. doi:10.2903/j.efsa.2023.8191

6. Bi Y, Li J, Shi W. The time is now: a call to contain H9N2 avian influenza viruses. The Lancet Microbe. 2022; S2666524722002324. doi:10.1016/s2666-5247(22)00232-4

7. Koopmans M, Wilbrink B, Conyn M, Natrop G, van der Nat H, Vennema H, et al. Transmission of H7N7 avian influenza A virus to human beings during a large outbreak in commercial poultry farms in the Netherlands. Lancet. 2004;363: 587–593. doi:10.1016/S0140-6736(04)15589-X

8. Pu J, Wang S, Yin Y, Zhang G, Carter RA, Wang J, et al. Evolution of the H9N2 influenza genotype that facilitated the genesis of the novel H7N9 virus. P Natl Acad Sci USA. 2015;112: 548–553. doi:10.1073/pnas.1422456112

9. Pu J, Yin Y, Liu J, Wang X, Zhou Y, Wang Z, et al. Reassortment with Dominant Chicken H9N2 Influenza Virus Contributed to the Fifth H7N9 Virus Human Epidemic. J Virol. 2021;95: e01578-20. doi:10.1128/JVI.01578-20

10. Chen H, Yuan H, Gao R, Zhang J, Wang D, Xiong Y, et al. Clinical and epidemiological characteristics of a fatal case of avian influenza A H10N8 virus infection: a descriptive study. Lancet. 2014;383: 714–721. doi:10.1016/S0140-6736(14)60111-2

11. Bi Y, Chen Q, Wang Q, Chen J, Jin T, Wong G, et al. Genesis, Evolution and Prevalence of H5N6 Avian Influenza Viruses in China. Cell Host & Microbe. 2016;20: 810–821. doi:10.1016/j.chom.2016.10.022

554 12. Qi X, Qiu H, Hao S, Zhu F, Huang Y, Xu K, et al. Human infection with an avian-origin
555 influenza A(H10N3) virus. N Engl J Med. 2022;386: 1087–1088.
556 doi:10.1056/nejmc2112416

557 13. Bao P, Liu Y, Zhang X, Fan H, Zhao J, Mu M, et al. Human infection with a reassortment
558 avian influenza A H3N8 virus: an epidemiological investigation study. Nat Commun.
559 2022;13: 6817. doi:10.1038/s41467-022-34601-1

560 14. Li C, Yu K, Tian G, Yu D, Liu L, Jing B, et al. Evolution of H9N2 influenza viruses from
561 domestic poultry in Mainland China. Virology. 2005;340: 70–83.
562 doi:10.1016/j.virol.2005.06.025

563 15. Peacock TP, James J, Sealy JE, Iqbal M. A global perspective on H9N2 avian influenza
564 virus. Viruses. 2019;11: 620. doi:10.3390/v11070620

565 16. Elgendy EM, Arai Y, Kawashita N, Isobe A, Daidoji T, Ibrahim MS, et al. Double
566 mutations in the H9N2 avian influenza virus PB2 gene act cooperatively to increase viral
567 host adaptation and replication for human infections. Journal of General Virology.
568 2021;102. doi:10.1099/jgv.0.001612

569 17. Gao Y, Zhang Y, Shinya K, Deng G, Jiang Y, Li Z, et al. Identification of amino acids in
570 HA and PB2 critical for the transmission of H5N1 avian influenza viruses in a mammalian
571 host. PLoS Pathog. 2009;5: e1000709. doi:10.1371/journal.ppat.1000709

572 18. Arai Y, Kawashita N, Hotta K, Hoang PVM, Nguyen HLK, Nguyen TC, et al. Multiple
573 polymerase gene mutations for human adaptation occurring in Asian H5N1 influenza virus
574 clinical isolates. Sci Rep. 2018;8: 13066. doi:10.1038/s41598-018-31397-3

575 19. Zaraket H, Baranovich T, Kaplan BS, Carter R, Song M-S, Paulson JC, et al. Mammalian
576 adaptation of influenza A(H7N9) virus is limited by a narrow genetic bottleneck. Nat
577 Commun. 2015;6: 6553. doi:10.1038/ncomms7553

578 20. Long JS, Mistry B, Haslam SM, Barclay WS. Host and viral determinants of influenza A
579 virus species specificity. Nat Rev Microbiol. 2019;17: 67–81.
580 doi:10.1038/s41579-018-0115-z

581 21. Camacho-Zarco AR, Kalayil S, Maurin D, Salvi N, Delaforge E, Milles S, et al. Molecular
582 basis of host-adaptation interactions between influenza virus polymerase PB2 subunit and
583 ANP32A. Nat Commun. 2020;11: 3656. doi:10.1038/s41467-020-17407-x

584 22. Carrique L, Fan H, Walker AP, Keown JR, Sharps J, Staller E, et al. Host ANP32A
585 mediates the assembly of the influenza virus replicase. Nature. 2020;587: 638–643.
586 doi:10.1038/s41586-020-2927-z

587 23. Long JS, Giotis ES, Moncorgé O, Frise R, Mistry B, James J, et al. Species difference in
588 ANP32A underlies influenza A virus polymerase host restriction. Nature. 2016;529:
589 101–104. doi:10.1038/nature16474

590 24. Subbarao EK, London W, Murphy BR. A single amino acid in the PB2 gene of influenza A
591 virus is a determinant of host range. J Virol. 1993;67: 1761–1764.

592 25. Zhang H, Zhang Z, Wang Y, Wang M, Wang X, Zhang X, et al. Fundamental contribution
593 and host range determination of ANP32A and ANP32B in influenza A virus polymerase
594 activity. J Virol. 2019;93: e00174-19. doi:10.1128/jvi.00174-19

595 26. Briggs K, Kapczynski DR. Comparative analysis of PB2 residue 627E/K/V in H5 subtypes
596 of avian influenza viruses isolated from birds and mammals. Frontiers in Veterinary
597 Science. 2023;10. doi:10.3389/fvets.2023.1250952

598 27. Hatta M, Hatta Y, Kim JH, Watanabe S, Shinya K, Nguyen T, et al. Growth of H5N1
599 influenza A viruses in the upper respiratory tracts of mice. PLoS Pathog. 2007;3: e133.
600 doi:10.1371/journal.ppat.0030133

601 28. Mistry B, Long JS, Schreyer J, Staller E, Sanchez-David RY, Barclay WS. Elucidating the
602 Interactions between Influenza Virus Polymerase and Host Factor ANP32A. J Virol.
603 2020;94: e01353-19. doi:10.1128/jvi.01353-19

604 29. Braun KM, Moreno GK, Halfmann PJ, Hodcroft EB, Baker DA, Boehm EC, et al.
605 Transmission of SARS-CoV-2 in domestic cats imposes a narrow bottleneck. PLoS Pathog.
606 2021;17: e1009373. doi:10.1371/journal.ppat.1009373

607 30. Moncla LH, Bedford T, Dussart P, Horm SV, Rith S, Buchy P, et al. Quantifying
608 within-host diversity of H5N1 influenza viruses in humans and poultry in Cambodia. PLoS
609 Pathog. 2020;16: e1008191. doi:10.1371/journal.ppat.1008191

610 31. Yang R, Sun H, Gao F, Luo K, Huang Z, Tong Q, et al. Human infection of avian influenza
611 a H3N8 virus and the viral origins: a descriptive study. The Lancet Microbe. 2022;3:
612 e824–e834. doi:10.1016/s2666-5247(22)00192-6

613 32. Sun H, Li H, Tong Q, Han Q, Liu J, Yu H, et al. Airborne transmission of human-isolated
614 avian H3N8 influenza virus between ferrets. Cell. 2023;0. doi:10.1016/j.cell.2023.08.011

615 33. Liu WJ, Li J, Zou R, Pan J, Jin T, Li L, et al. Dynamic PB2-E627K substitution of influenza
616 H7N9 virus indicates the in vivo genetic tuning and rapid host adaptation. : 8.
617 doi:10.1073/pnas.2013267117

618 34. Zhu Z, Fodor E, Keown JR. A structural understanding of influenza virus genome
619 replication. Trends in Microbiology. 2023;31: 308–319. doi:10.1016/j.tim.2022.09.015

620 35. Baker SF, Ledwith MP, Mehle A. Differential splicing of ANP32A in birds alters its ability
621 to stimulate rna synthesis by restricted influenza polymerase. Cell Rep. 2018;24:
622 2581-2588.e4. doi:10.1016/j.celrep.2018.08.012

623 36. Taft AS, Ozawa M, Fitch A, Depasse JV, Halfmann PJ, Hill-Batorski L, et al. Identification
624 of mammalian-adapting mutations in the polymerase complex of an avian H5N1 influenza
625 virus. Nature Communications. 2015;6. doi:10.1038/ncomms8491

626 37. Chin AWH, Li OTW, Mok CKP, Ng MKW, Peiris M, Poon LLM. Influenza A viruses with
627 different amino acid residues at PB2-627 display distinct replication properties in vitro and
628 in vivo: revealing the sequence plasticity of PB2-627 position. Virology. 2014;0: 545–555.
629 doi:10.1016/j.virol.2014.09.008

630 38. Arai Y, Kawashita N, Ibrahim MS, Elgendy EM, Daidoji T, Ono T, et al. PB2 mutations
631 arising during H9N2 influenza evolution in the Middle East confer enhanced replication
632 and growth in mammals. PLoS Pathog. 2019;15: e1007919.
633 doi:10.1371/journal.ppat.1007919

634 39. Li X, Shi J, Guo J, Deng G, Zhang Q, Wang J, et al. Genetics, receptor binding property,
635 and transmissibility in mammals of naturally isolated H9N2 avian influenza viruses. PLoS
636 Pathog. 2014;10: e1004508. doi:10.1371/journal.ppat.1004508

637 40. Carnaccini S, Perez DR. H9 influenza viruses: an emerging challenge. Cold Spring Harb
638 Perspect Med. 2020;10: a038588. doi:10.1101/cshperspect.a038588

639 41. Sun X, Belser JA, Maines TR. Adaptation of H9N2 influenza viruses to mammalian hosts:
640 a review of molecular markers. Viruses. 2020;12: 541. doi:10.3390/v12050541

641 42. Sun Y, Pu J, Jiang Z, Guan T, Xia Y, Xu Q, et al. Genotypic evolution and antigenic drift of
642 H9N2 influenza viruses in China from 1994 to 2008. Vet Microbiol. 2010;146: 215–225.
643 doi:10.1016/j.vetmic.2010.05.010

644 43. Xu G, Zhang X, Gao W, Wang C, Wang J, Sun H, et al. Prevailing PA mutation K356R in
645 avian influenza H9N2 virus increases mammalian replication and pathogenicity. Journal of
646 Virology. 2016;90: 8105–8114. doi:10.1128/jvi.00883-16

647 44. Gao W, Zu Z, Liu J, Song J, Wang X, Wang C, et al. Prevailing I292V PB2 mutation in
648 avian influenza H9N2 virus increases viral polymerase function and attenuates IFN-β
649 induction in human cells. J Gen Virol. 2019;100: 1273–1281. doi:10.1099/jgv.0.001294

650 45. Xiao C, Ma W, Sun N, Huang L, Li Y, Zeng Z, et al. PB2-588 V promotes the mammalian
651 adaptation of H10N8, H7N9 and H9N2 avian influenza viruses. Sci Rep-UK. 2016;6:
652 19474. doi:10.1038/srep19474

653 46. Edgar RC. MUSCLE: a multiple sequence alignment method with reduced time and space
654 complexity. BMC Bioinformatics. 2004;5: 113. doi:10.1186/1471-2105-5-113

655 47. Miller MA, Pfeiffer W, Schwartz T. Creating the cipres science gateway for inference of
656 large phylogenetic trees. 2010 Gateway Computing Environments Workshop (GCE). 2010.
657 pp. 1–8. doi:10.1109/gce.2010.5676129

48. Chen C, Wu Y, Li J, Wang X, Zeng Z, Xu J, et al. TBtools-II: A “one for all, all for one” bioinformatics platform for biological big-data mining. Molecular Plant. 2023;16: 1733–1742. doi:10.1016/j.molp.2023.09.010

49. Su YCF, Bahl J, Joseph U, Butt KM, Peck HA, Koay ESC, et al. Phylodynamics of H1N1/2009 influenza reveals the transition from host adaptation to immune-driven selection. Nat Commun. 2015;6: 7952. doi:10.1038/ncomms8952

50. Hernandez R, Brown DT. Growth and maintenance of chick embryo fibroblasts (CEF). Curr Protoc Microbiol. 2010;Appendix 4: 4I. doi:10.1002/9780471729259.mca04is17

51. Zhang P, Tang Y, Liu X, Liu W, Zhang X, Liu H, et al. A novel genotype H9N2 influenza virus possessing human H5N1 internal genomes has been circulating in poultry in eastern china since 1998. J Virol. 2009;83: 8428–8438. doi:10.1128/jvi.00659-09

52. Belser JA, Eckert AM, Huynh T, Gary JM, Ritter JM, Tumpey TM, et al. A guide for the use of the ferret model for influenza virus infection. The American Journal of Pathology. 2020;190: 11–24. doi:10.1016/j.ajpath.2019.09.017

674 **Figures and Tables**

675 **Fig 1 Emergence and cross-host species function of PB2-627V.**

676 (**A).** The global prevalence of PB2-627V in influenza A viruses (IAVs) (excluding human H3N2
677 and H1N1pdm09 viruses) during 1994-2022. Bars show the number of isolates by subtype and
678 host, while a world map displays the isolate's number by location. (**B).** Phylogenetic tree of PB2
679 genes with the residue 627V collected worldwide during 1994-2022 (n=394). Human isolates'
680 names are in red. (**C).** Amino acid polymorphisms of the PB2-627 residue in avian and
681 human-derived H9N2 viruses isolated in China. All sequence data were collected from the
682 GISAID database**.** (**D-E)**. Relative polymerase activities at 33°C or 37°C. DF-1 cells **(D)** and
683 293T cells **(E)** were transfected with firefly minigenome reporter, renilla expression control, and
684 polymerase (PB2, PB1, PA, and NP) of 17/H9N2^{627E}, 17/H9N2^{627V}, or 17/H9N2^{627K}. Cells were
685 incubated for 24 hours and the luciferase activities, normalized to corresponding renilla
686 luciferase activity, are presented relative to 17/H9N2^{627E} (set as 1). Each data point is the mean ±
687 SD of three independent experiments (one-way ANOVA). **(F).** Heat map shows p-values of
688 polymerase activities in DKO cells overexpressing ANP32 proteins. chANP32A, chANP32B,
689 huANP32A, huANP32B, or empty vector was transfected into DKO cells, incubated at 33°C and
690 37°C for 24 hours, and assayed the luciferase activity. Statistical significance was based on
691 one-way ANOVA and subsequent Dunnett's test, compared with the corresponding value of
692 empty vector (ns, not significant; *, $p<0.05$; **, $p<0.01$; ***, $p<0.001$). (**G).** Impact of amino
693 acids at the PB2-627 position on the surface charge of the PB2 protein. Red (negative) and blue
694 (positive) proteins are shown.

695 **Fig 2. PB2-627V conferred dual adaptability to H9N2 virus to replicate in avian and**
696 **mammalian species.**

697 (**A).** CEF cells were infected with indicated viruses at 0.01 MOI and virus titers were determined
698 at indicated times post-infection by $TCID_{50}$ assays. (**B-D).** Groups of 6 chickens were i.n.
699 infected with indicated viruses at 10^6 EID_{50}, three chickens from each group were used to
700 determine the viral titers (**B**) from oropharyngeal samplings at 2, 4, 6, and 8 dpi. Another three
701 chickens from each group were euthanized at 3 dpi. Virus titers (**C**) of the turbinates and lungs
702 were determined. Representative histopathological findings (**D**) in the lungs of infected mice.
703 Lung sections were stained with H&E (upper) and by IHC against influenza viral NP antigen
704 (lower). Scale bars, 100 mm. (**E).** A549 cells were infected with indicated viruses at 0.1 MOI
705 and virus titers were determined by $TCID_{50}$ assays at indicated times post-infection. (**F-H).**
706 Groups of 8 mice were infected with the indicated virus at doses of 10^6 $TCID_{50}$. Five mice of
707 each group were monitored for body weight changes (**F**) over 14 days. Additional three mice
708 from each group at 3 dpi were euthanized. Virus titers (**G**) in the turbinates and lungs were
709 determined by $TCID_{50}$ assays. Representative histopathological findings (**H**) in the lungs of
710 infected mice. Lung sections were stained with H&E (upper) and by IHC against influenza viral
711 NP antigen (lower). Scale bars, 100 mm. Data are represented as mean ± SD. Statistical
712 significance was based on two-way ANOVA, compared with the corresponding value of
713 $17/H9N2^{627E}$ (ns, not significant; *, $p < 0.05$; **, $p < 0.01$; ***, $p < 0.001$).

714 **Fig 3 PB2-627V facilitated aerosol transmissibility of H9N2 virus in ferrets.**

715 Each ferret (n = 3) was inoculated with 10^6 $TCID_{50}$ of indicated virus. The next day, the infected
716 ferret was individually paired by co-housing with a DC ferret; an RD-contact ferret was also
717 housed in a wire frame cage adjacent to the infected ferret. Nasal washes were collected for
718 virus-shedding detection every other day from all ferrets from 2 dpi. (**A-C).** Virus titers of nasal
719 washes were determined by $TCID_{50}$ assays on MDCK cells. Each color bar represents virus titers

720 of an individual ferret. Dashed lines indicate the lower limit of virus detection ($10^{1.5}$ $TCID_{50}$/ml).
721 (**D).** AUC values approximate total virus output throughout infection (mean AUC from three
722 ferrets). (**E-G).** For each infected or transmitted ferret, the nasal washes collected at the first and
723 last virus detection time were analyzed by deep sequencing. Detection time points are based on
724 the results shown in Fig. 3, A-C. The height of each letter indicates the relative ratio of amino
725 acids at PB2-627. Sequencing was performed on an Illumina NovaSeq platform.

726 **Fig 4 PB2-627V has the potential for sustained prevalence in poultry.**

727 **(A).** Schematic depiction of virus passage in chickens**.** Groups of 2 chickens were each i.n.
728 infected with 10^6 $TCID_{50}$ of indicated virus (P1), and subsequently passaged (P1-P5) by contact.
729 (**B).** Intra-host single nucleotide variants (iSNVs) frequency of P5 chicken. Variants of
730 nucleotide site detected above 1% threshold were identified as iSNVs. All iSNVs were further
731 determined as high-frequency (>10%) and low-frequency (≤10%). iSNVs frequency of the whole
732 genome was calculated by using the number of iSNVs divided by the total number of genome
733 sites. iSNVs frequency was expressed as the log. (**C)**. Variant frequency nucleotides encoding
734 PB2-627 residue. The height of each letter indicates the average ratio of nucleotides encoding
735 PB2-627 residue in two samples of each group. (**D)**. Graphs represent all iSNVs detected in P5
736 chicken. Variant frequencies are plotted by genome location and are colored by virus groups. two
737 high-frequency non-synonymous iSNVs are circled and labeled with the corresponding amino
738 acid mutations. Yellow backgrounds depict RNP genes (PB2, PB1, PA, and NP). Sequencing
739 was performed on an Illumina NovaSeq platform. Data are presented as mean ± SD. Statistical
740 significance was based on two-way ANOVA (ns, not significant, *, $p < 0.05$; **, $p < 0.01$; ***, p
741 < 0.001).

742 **Fig 5 PB2-627V conferred dual adaptability in avian H7N9 and H3N8 viruses to replicate**
743 **in chickens and mice.**
744 **(A-E).** Groups of 6 chickens were infected with indicated viruses at doses of 10^6 EID_{50}. Three
745 infected chickens in each group were monitored for survival (**A**, **C)** over 14 days. At 3 dpi, the
746 other three chickens in each group were euthanized. Virus titers (**B**, **D**) in the turbinates and
747 lungs were determined by $TCID_{50}$ assays. Representative histopathological findings (**E**) in the
748 lungs of infected mice. Lung sections were stained with H&E (left) and by IHC against influenza
749 viral NP antigen (right). Scale bars, 100 mm. (**F-L).** Groups of 8 mice were infected with
750 indicated viruses at doses of 10^6 $TCID_{50}$. Five mice in each group were monitored for survival (**F**,
751 **I**) and body weight changes (**G**, **J**) over 14 days. Mortality from infection included mice
752 euthanized at a weight loss of 25% or more. At 3 dpi, the other three mice in each group were
753 euthanized. Virus titers (**H**, **K**) in the turbinates and lungs were determined by $TCID_{50}$ assays.
754 Representative histopathological findings (**L**) in the lungs of infected mice. Lung sections were
755 stained with H&E (left) and by IHC against influenza viral NP antigen (right). Scale bars, 100
756 mm. Data presented are represented as mean ± SD. Statistical significance was based on
757 two-way ANOVA (ns, not significant; *, $p < 0.05$; **, $p < 0.01$; ***, $p < 0.001$).

758 # Supporting information

759 **S1 Fig. H9N2 virus and its reassortants with PB2-627V are in the same cluster. (A).** A total
760 of 4523 H9N2 PB2 sequences were collected from GISAID, Amino acid at PB2-627 residue and
761 the location of all isolates are shown. **(B).** The MCC tree of the PB2-627V cluster. The internal
762 nodes indicated the most recent common ancestor of the sub-group, which is divided into avian
763 and human. All human strains' names are in bold.

764 **S2 Fig. Increased detection of PB2-627V in novel AIVs reassortant with H9N2 PB2 gene**
765 **since 2016.** All the sequences of H7N9, H5N6, H10N3 and H3N8 PB2 genes were obtained
766 from the GISAID database. Viruses with PB2 gene identity greater than 97% to that of PB2 gene
767 of H9N2 viruses were considered reassortants of H9N2. The bars depict the number of isolates
768 with PB2-627V in different subtypes and hosts before and after 2016.

769 **S3 Fig. Host ANP32 required for viral polymerase and differential viral RNA production in**
770 **avian and human cells. (A, B).** DF-1 cells **(A)** and A549 cells **(B)** were infected with indicated
771 viruses at MOI of 0.001 and 0.1 respectively. The cells were cultured at 37℃ for 24 hours after
772 infection. PB2 mRNA and vRNA, normalized to β-actin expression, determined by quantitative
773 real-time PCR. **(C).** Wild-type 293T cells and DKO cells were transfected with firefly
774 minigenome reporter, renilla expression control, and polymerase genes of 17/H9N2^{627E},
775 17/H9N2^{627V}, or 17/H9N2^{627K}. The cells were cultured at 37℃ for 24 hours after transfection.
776 Data indicate the firefly luciferase gene activity normalized to the renilla luciferase gene activity.
777 Statistical differences between samples are indicated, based on one-way ANOVA with Dunnett's
778 testing (ns, not significant; *, $p < 0.05$; **, $p < 0.01$; ***, $p < 0.001$). Error bars are SEM in one
779 representative experiment.

780 **S4 Fig. Survival of infected mice and chickens. (A)**. Groups of 3 chickens were i.n. infected
781 with indicated viruses at 10^6 EID_{50}, and the survival were monitored for 14 days. **(B).** Groups of
782 5 mice were infected with indicated virus at doses of 10^6 $TCID_{50}$ and the survival were monitored
783 for 14 days.

784 **S5 Fig. H&E and IHC of chicken and mouse lungs infected with PB2-627 variant H3N8**
785 **viruses. (A).** Chickens were infected at 10^6 EID_{50} with indicated viruses, and three chickens per
786 group were euthanized at 3 dpi. **(B).** Mice were infected at 10^6 $TCID_{50}$ with indicated viruses,

787 and three mice per group were euthanized at 3 dpi. Lung sections were stained with H&E and
788 subjected IHC for the detection of viral NP protein. Scale bars, 100 μm.

789 **S1 Table. Hosts, geographical distribution, and subtypes of AIVs carrying PB2-627V.**

790 **S2 Table. Clinical symptoms of ferrets infected with H9N2 influenza viruses**

791 **S3 Table. Area under the curve (AUC) values of virus output of infected/exposed ferrets**

792

793

794

795

796

797

798

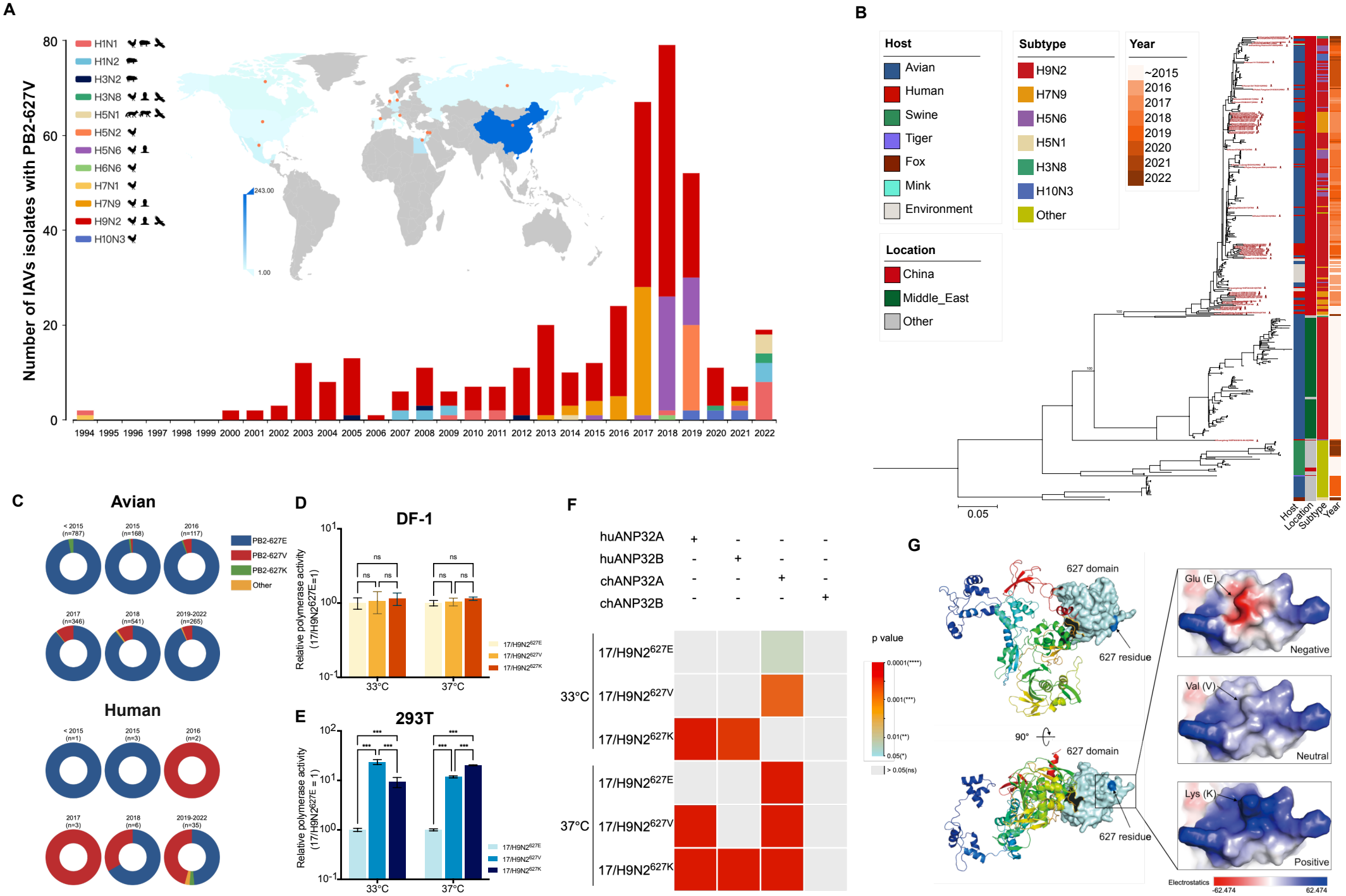

Fig 1. Emergence and cross-host polymerase activity of PB2-627V

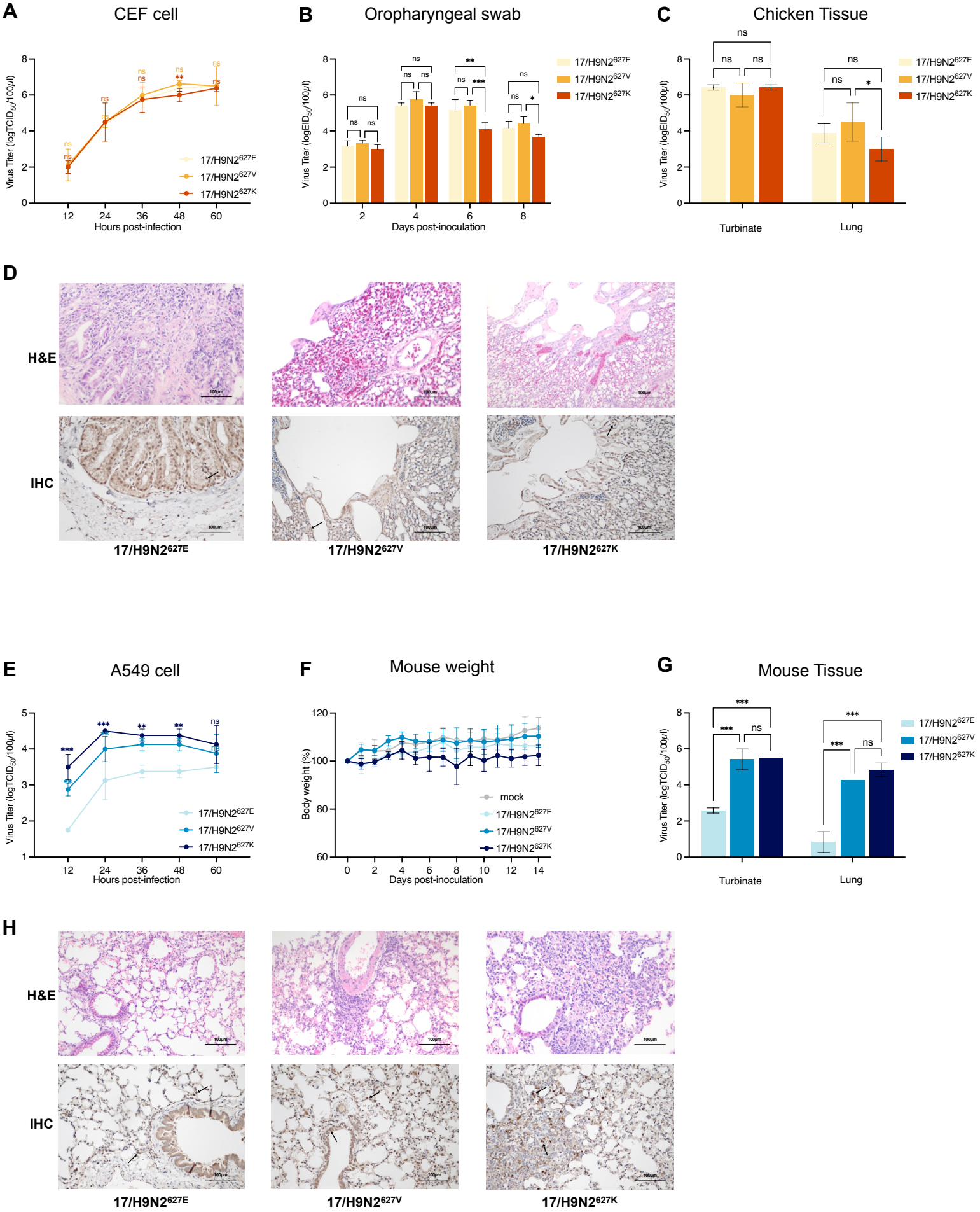

Figure 2. PB2-627V conferred dual adaptability to H9N2 virus to replicate in avian and mammalian species.

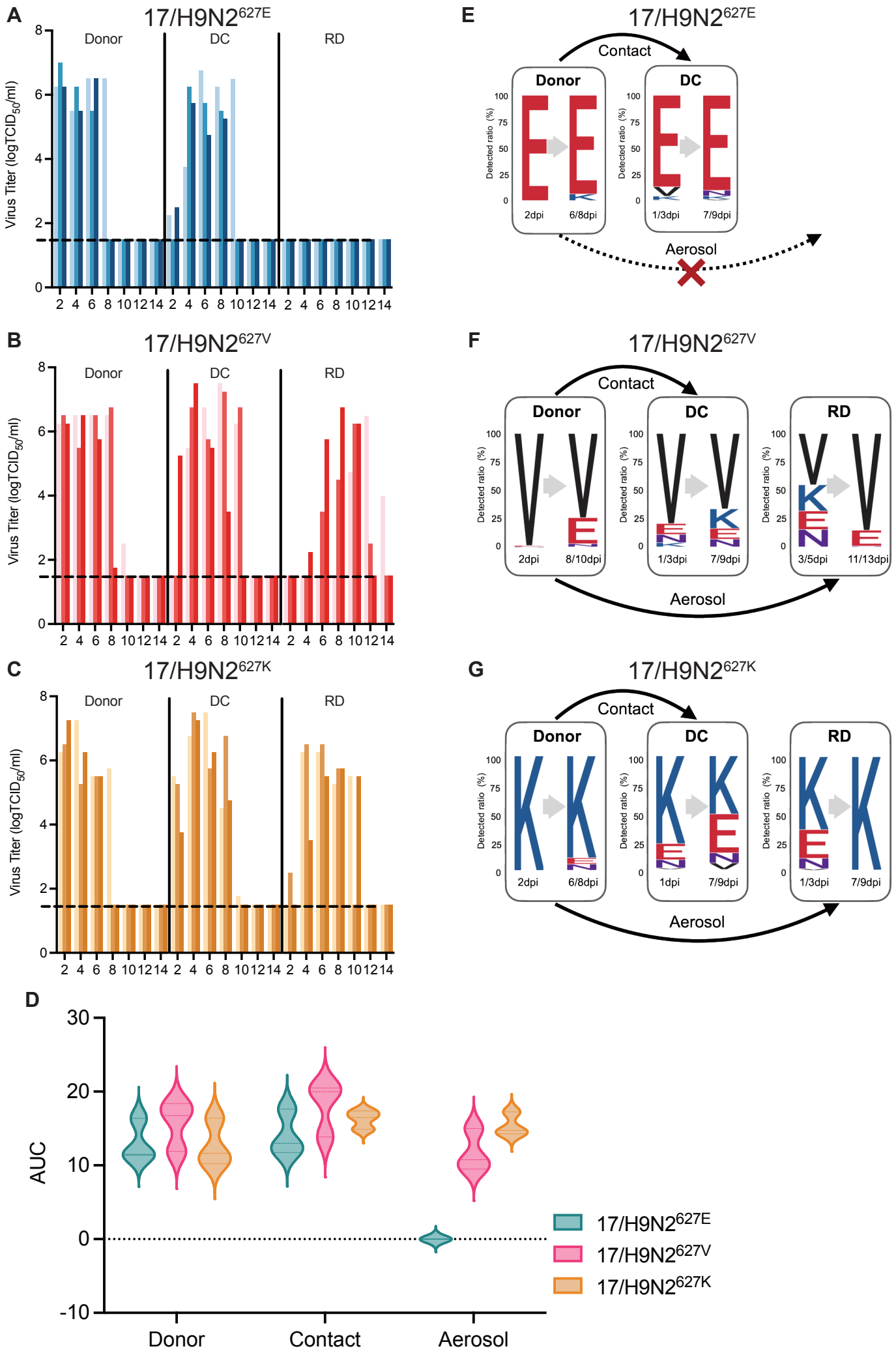

Fig 3. PB2-627V facilitated aerosol transmissibility of H9N2 virus in ferrets

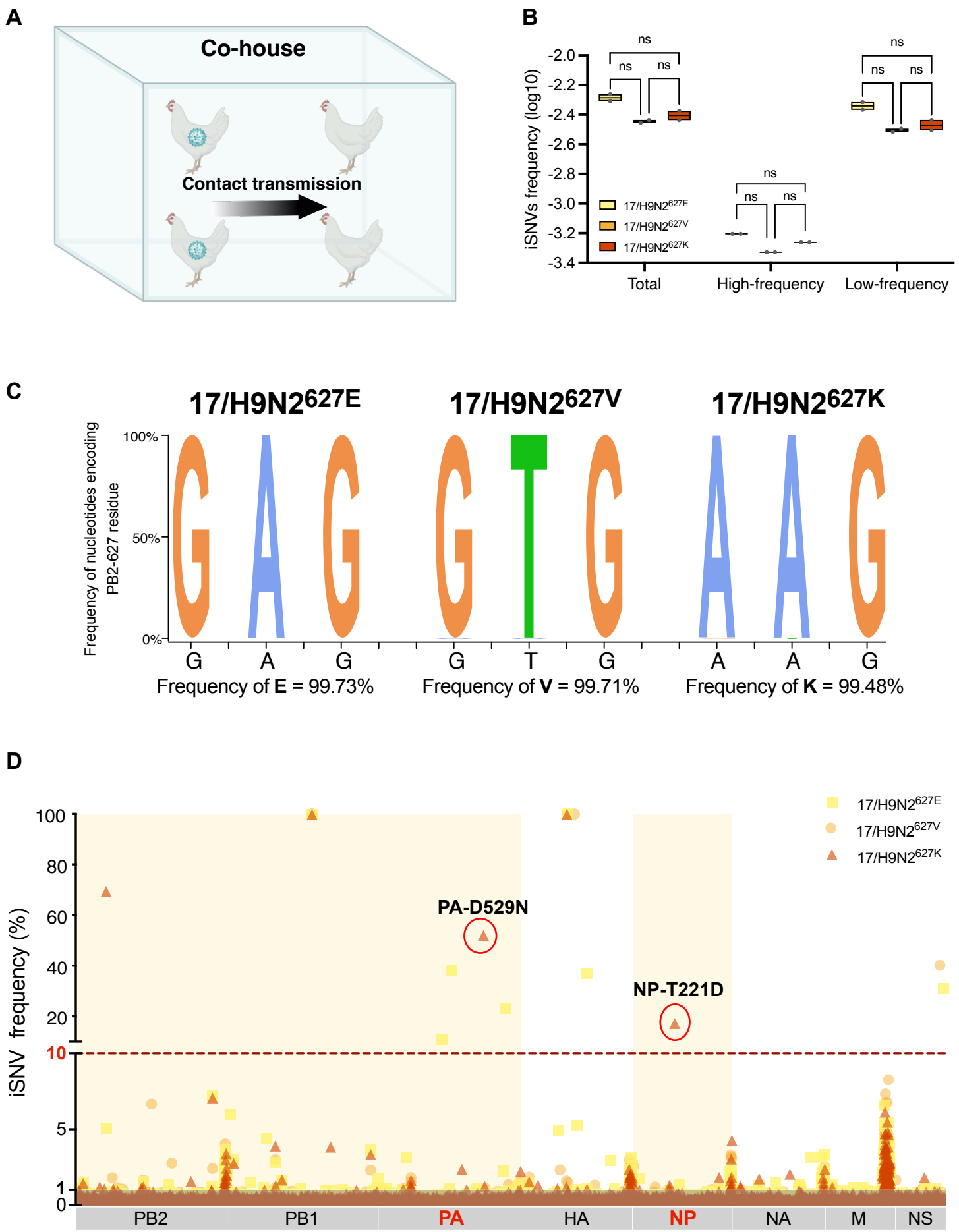

Fig 4. PB2-627V has the potential for sustained prevalence in poultry

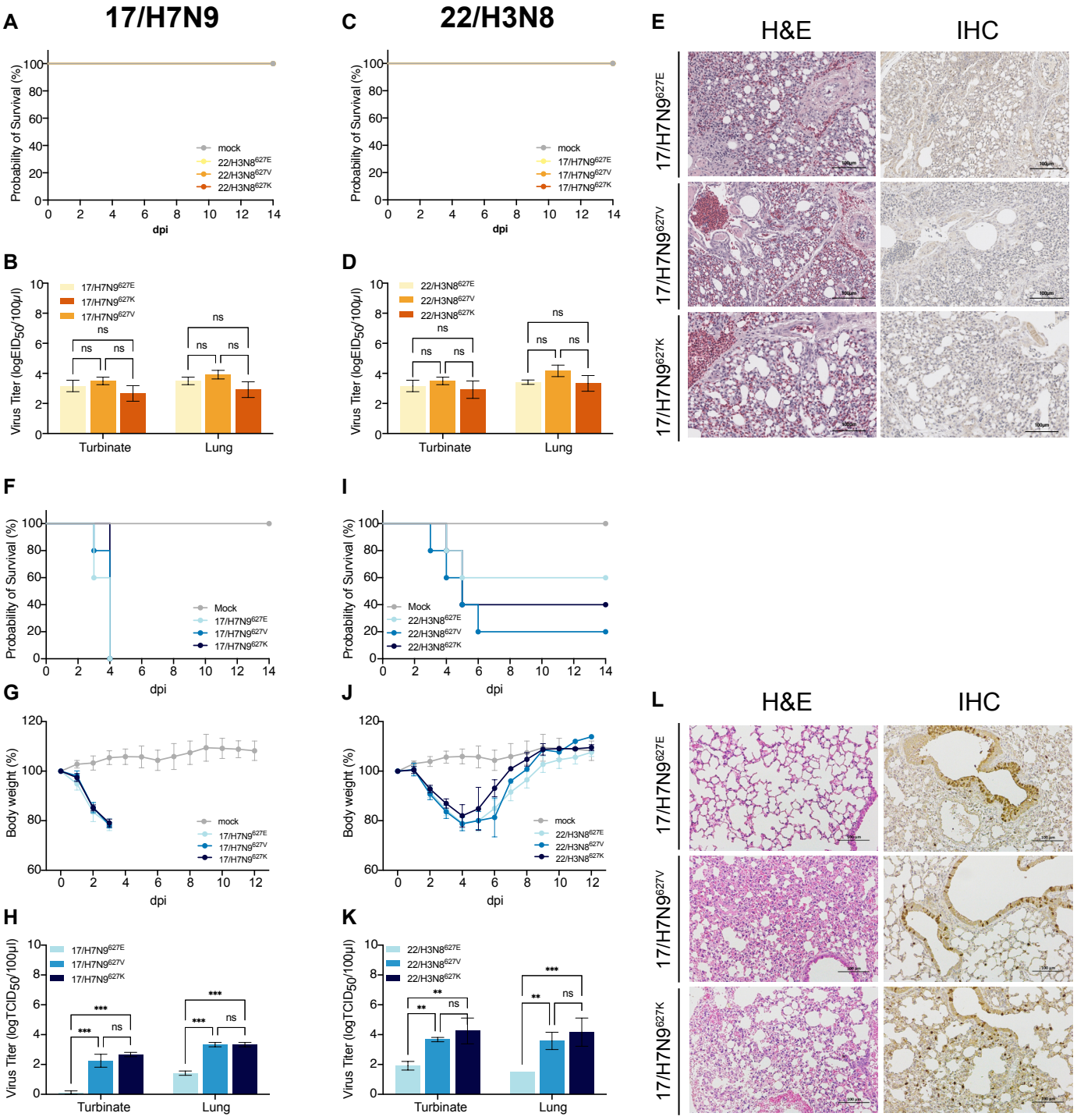

Fig 5. PB2-627V conferred dual adaptability in avian H7N9 and H3N8 viruses to replicate in chickens and mice